The ballistic wave, from rifle bullet to Apollo command module

J. Varnier, F. Sourgen

The ballistic wave, from rifle bullet to Apollo command module

Jean Varnier and Frédéric Sourgen
ONERA, Dept. DSNA / Dept. DMAE, France
Corresponding Author: jean.varnier@onera.fr

PACS: 43.25.Cb, 43.28.Mw

ABSTRACT

The ballistic wave is a shaking generated by a solid body moving at supersonic velocity in the atmosphere. To human hearing, it is heard as a crack for small projectiles, as a detonation (sonic boom) for large-sized bodies. Their common signature is an N-shaped profile giving pressure in function of time, the formalism of which is known. But this formalism presents a practical difficulty, namely the calculation of a "volume function" for the mobile in question: we present an option for that calculation in the classical case of projectiles shot from small-calibre firearms (Camp Irwin, California, USA, 1944). Besides, that formalism has to be adapted for any object the diameter of which is bigger than length, which is the case of the Apollo Command Module during its reentry into the atmosphere above the Pacific Ocean. Measurements of sonic boom were carried out aboard US Navy ships during reentries of Apollo 15 and Apollo 16 Command Modules. These measurements constitute a very interesting data base in order to test, in cases of high altitude and high Mach number, the results given by a model of fluid mechanics and a model of nonlinear propagation in the one hand, by an analytical semi-empirical model on the other hand.

1. INTRODUCTION

The ballistic wave generated by a projectile moving at supersonic velocity was the subject of experimental studies from the end of 19th century and the beginning of 20th Century [1-2]. A semi-empirical theory enabling to calculate this shock wave was developed during World War II and after this war [3-6]. The theory was later extended to aircraft in order to foreknow the intensity of sonic boom, for instance when supersonic jets such as the French airliner *Concorde* or the USAF's strategic reconnaissance plane SR-71 *Blackbird* were put into service [7-9]. However, small-calibre projectiles are the subject of recent studies, in mind for their operational detection and location [10-11]. On the other hand, the sonic boom generated by solid bodies entering the upper atmosphere was the subject of experimental studies [12-13]. In this case, classic physical models are on the very borderline of their application domain. We are interested in those uppermost cases that are in fact simulated by the same semi-empirical code. The study is completed by computations performed with the help of the ONERA's CFD code CEDRE, giving pressure and velocity profiles around the Apollo Command Module moving at high altitude and at high Mach number.

2. BALLISTIC WAVE OF A PROJECTILE

2.1. Theory

For human hearing, the ballistic wave generated in the atmosphere by a body such as a rifle bullet moving at supersonic speed (Fig. 1) is perceived as a sharp snap similar to a whip crack when the projectile is passing by. The wave corresponds to a shock wave bordered with a sudden overpressure in front of the wave and a sudden underpressure at its rear part, hence the generic denomination "N-wave" given to the time signal (see Fig. 2, on the left). This profile can be characterized by two parameters: pressure amplitude ΔP and going past duration ΔT. Their values at a given distance from the projectile path can be calculated with the help of a semi-empirical formalism [4-6]. Dimensions and shape of the projectile are introduced by the Whitham function (also called "volume function") the integral I_W of which, used in order to calculate ΔP and ΔT, is given by:

$$I_W = \int_0^L ds \, \frac{1}{2\pi} \int_0^S \frac{S''(x)}{\sqrt{s - x}} \, dx \qquad (1)$$

where S(x) is the cross-section of the mobile at abscissa x and L is its length (see Fig. 3), s being an integration parameter. It should be

noted that the complex formulas giving the values of ΔP and ΔT also refer to the Mach number of the mobile and to the ambient atmospheric conditions. In Ref. [11-12], Equation (1) is implicitly replaced by the following formula:

$$I_W = \frac{R^2}{\sqrt{L}} \qquad (2)$$

where R is the projectile radius and L its overall length. A calculation of I_W performed at the ONERA with the parabolic shape of the nose cone shown in Figure 3 leads to the same formula, aside the fact that L is replaced by the length H of the ogival part of the bullet. Moreover the calculation shows that a sharp shape of the nose (similar to that of Fig. 1) generated by an arc of parabola, R and H remaining unchanged, increases the value of I_W given by Equation (2) only slightly.

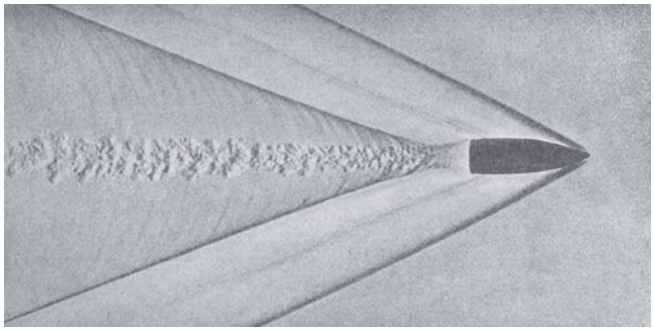

Figure 1. *Shock wake from a rifle bullet [2].*

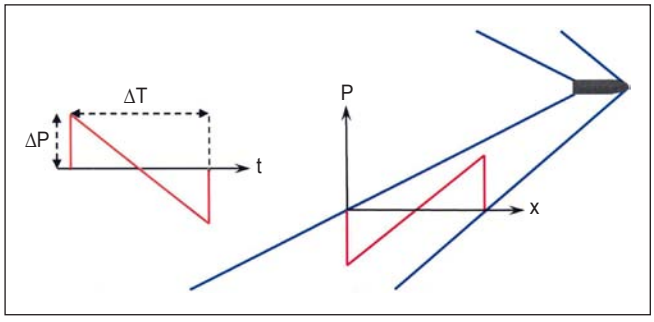

Figure 2. *Time profile and space profile of the N-wave.*

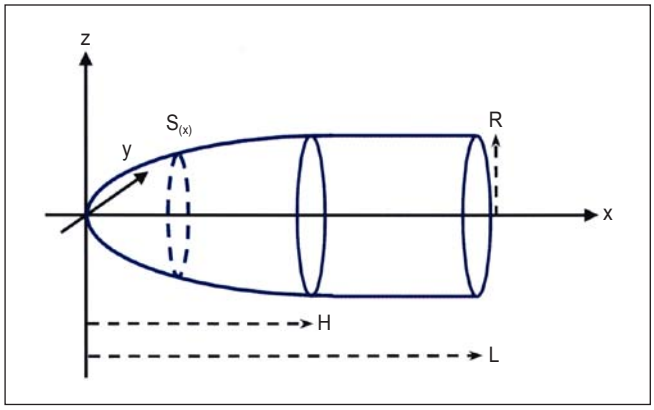

Figure 3. *Geometry of a projectile to calculate the Whitham function.*

2.2. Application

We refer to experimentations performed at Camp Irwin, California, in November 1944. They provided the data base used in Ref. [4]. The following calibres were tested: 7.62 mm (.30 inch), 12.7 mm (.50 inch), 20 mm and 40 mm. All these calibres were in standard service in U.S. Army at this time. Unhappily full test data are available for two calibres only, 12.7 mm and 40 mm. The study of corresponding firearms and ammunitions led us to consider the following initial velocities for projectiles: 880 m/s (Mach 2.58) for 12.7 mm calibre, 854 m/s (Mach 2.50) for 40 mm calibre. To perform the calculations, we have chosen the ambient pressure and temperature which correspond to the CIRA/COSPAR statistical atmosphere for the month of November, latitude 35° North, height 750 m over sea level. We have supposed that the fly-by speed of the projectiles during the experiments was roughly equal to their muzzle velocity.

The shapes of 12.7 mm bullet and of 40 mm shell are taken into account in order to calculate the values of integral (2) and of the theoretical parameters of the N-wave.

As experimental values of pressure peak ΔP and of fly-by duration ΔT of the ballistic wave, we adopt the averages determined by Du Mond et al. [4] out of several test shoots. It is important to notice that the amplitude ΔP is a datum less reliable than the duration ΔT for two reasons:

- at short distances, the nonlinear effects lead to an important decreasing in pressure according to the distance, a fact which is not reported by the far-field formalism used;
- Du Mond points out that there are sound reflection effects on the ground which are not quantified in his analysis.

These two types of effect tend to increase the amplitude of ballistic wave in comparison with theoretical calculation. In contrast, their influence on the ballistic wave duration seems to be negligible.

For the fly-by duration DT of the ballistic wave at various measurement distances, comparison of computed values to measured values (with use of the ONERA's code JAZZ that applies the Whitham's theory with some simplifications) is shown in Fig. 4 for two calibres, 12.7 mm and 40 mm. As a general rule, the similarity is very satisfactory, as it is also with calculations performed by Du Mond et al., who used a more or less similar formalism.

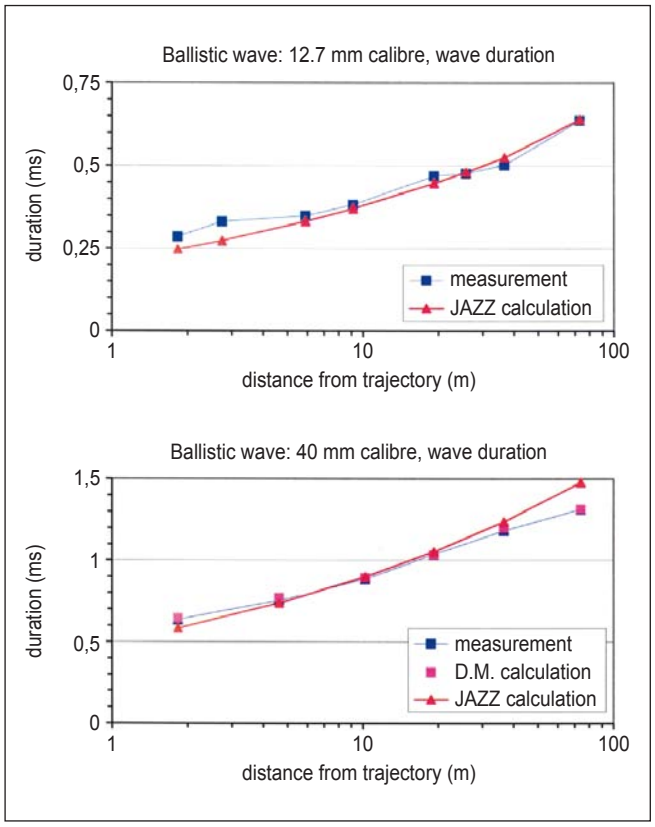

Figure 4. Comparison between computed and measured values for ΔT.

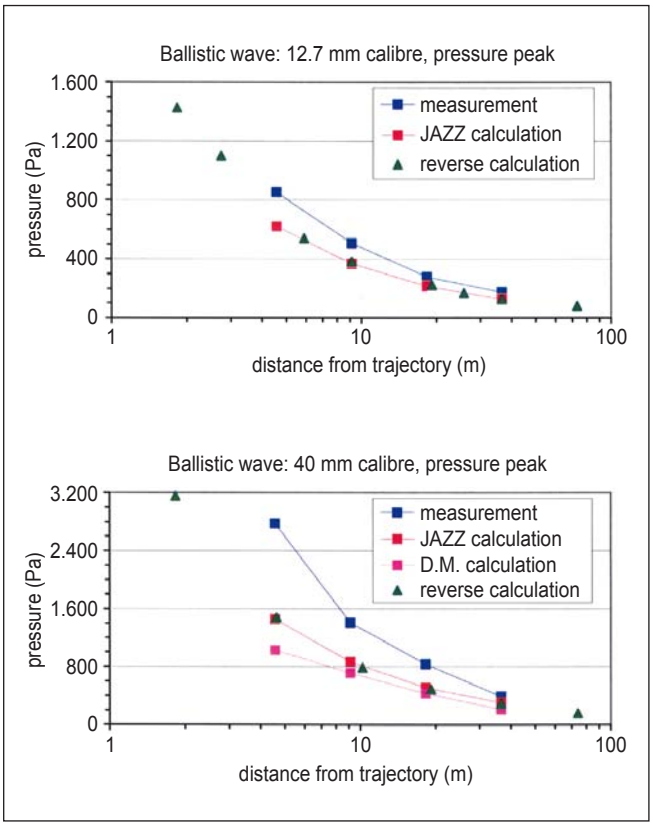

Figure 5. Comparison between computed and measured values for ΔP.

The same comparisons are done for the pressure peak ΔP in Fig. 5 - unhappily no reproduction of any actual recording is found in [4]. As expected, the differences between calculation and measurement are clearly greater, but we have to note that:

- these differences decrease when the distance increases;
- for the same distance, these differences are greater for the 40 mm calibre than for the 12.7 mm calibre.

The former remark is easy to explain by the decreasing of nonlinear effects, in particular decreasing of thermal dissipation, when we go away from the projectile path. The latter remark has the same cause, in relation with the calibre of projectiles to which the distances have to be related: thus 4 meters is equivalent to 315 calibres for the 12.7 mm bullet, but only to 100 calibres for the 40 mm shell.

We transferred to both Figures 5, linked up with calibres 12.7 mm and 40 mm respectively, the amplitudes calculated from the measured durations by the way of Equation (3) - so-called "reverse calculation". Obviously, it gets closer to simulations, because this calculation cancels both nonlinear effects and effects of reflection on the ground at once. Note that the ratio $\Delta T/\Delta P$ removes the common factor $I_W^{1/2}$ in the formalism, and therefore is independent of the geometry of the projectile. We have indeed after simplification:

$$\frac{\Delta T}{\Delta P} = \frac{2}{P_0}\frac{\gamma+1}{\gamma c_0}\frac{M}{\sqrt{M^2-1}}\,r \qquad (3)$$

where r is the distance to the bullet trajectory, M is the Mach number, P_0, c_0 and γ being ambient data (pressure, sound speed, air specific heat ratio).

3. SONIC BOOM OF APOLLO COMMAND MODULE

3.1. Simplified approach

The sonic boom of aircraft is a large-scale ballistic wave which is perceived as a violent detonation for human hearing, in particular if focusing occurs - do not confuse with the double-bang, the causes of which are different. The theory applied is identical to the theory of ballistic wave of projectiles, except the introduction of a "lift function" to take into account the effects of incidence, what increases the amplitude of the corresponding N-wave. Note that often a dissymmetry appears between the "positive" and "negative" parts of the amplitude: for instance, the Figure 6 shows the recording of a focused sonic boom due to the acceleration of an aircraft in horizontal flight [14].

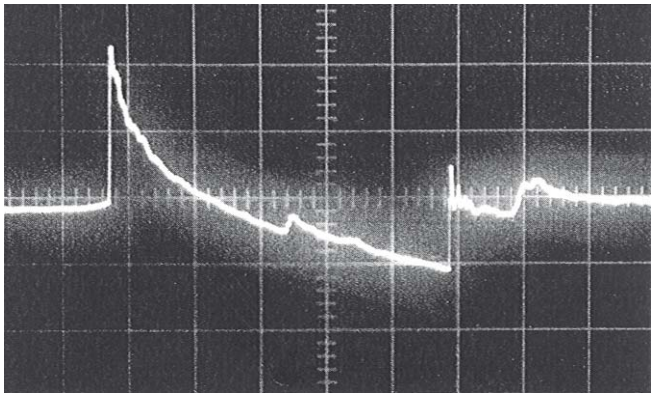

Figure 6. *Sonic boom from a fighter Mirage III [14].*

The case of sonic booms arisen from Apollo Command Modules during their reentry into the atmosphere above the Pacific Ocean [12-13] is different: indeed, velocities and altitudes have magnitude beyond usual limits of the model (Mach 3 at 26,000 m high at the most for SR-71), and a lift effect is generated by the incidence of the vehicle in reference to the velocity vector (about 20°). The problem that arises for the modelling is linked up to the particular shape of Apollo Command Module, a shape that has nothing in common with the one of a bullet or of an aircraft: 3.4 m high for 3.9 m in diameter (Fig. 7).

In order to calculate the Whitham's integral I_W for the heat shield, we suppose that its shape is generated by an arc of parabola: note that H replaces L in Equation (2).

On the other hand, some computations of fluid mechanics (ONERA's code ELSA) and of nonlinear propagation (NASA's code TRAPS [15]) concerning the influence of the length of a mobile on the N-wave duration DT showed that this duration had to be corrected by the following factor:

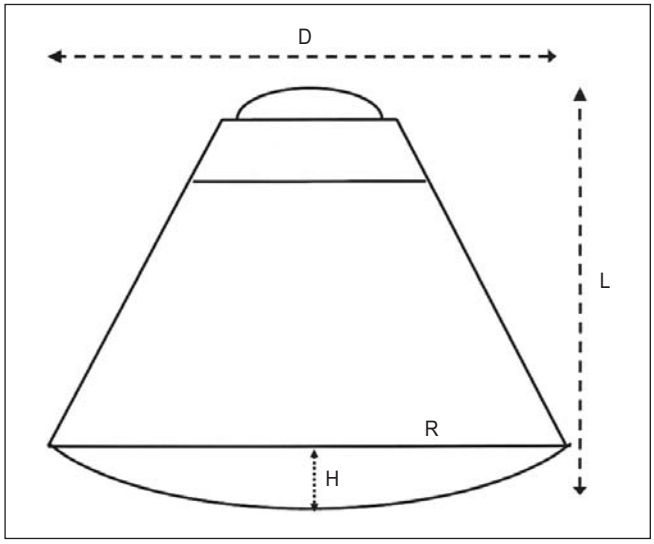

Figure 7. *Apollo Command Module [12].*

$$F_{(\Delta T)} = \left(\frac{L}{8D}\right)^{1/4} \quad (4)$$

where L is the overall length and D the diameter of the mobile.

Note that the value of this corrective factor would be close to one for the "slender body" which served as reference for the Whitham's theory [5], what can be accepted for firearm projectiles in general, because of the cap effect which widens the projectile wake (see Fig. 1).

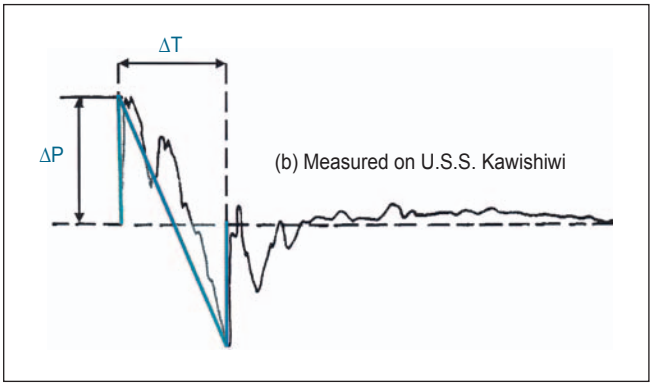

Figure 8. *Recorded sonic boom signal [12], equivalent N-wave.*

Moreover, a factor of reflected field equal to two has to be brought to amplitude ΔP when sensors are put on the ground, in this case the deck of US Navy's ships stationed under the reentry trajectory of the spacecraft.

The signals recorded on the ships have an irregular form very probably due to the reflection on the sea surface of the incident wave: see the double peak of "positive" and of "negative" pressure in Fig. 8. Following this hypothesis, parameters [ΔP, ΔT] of an equivalent N-wave were correctly determined in the NASA's papers.

The Whitham's formalism is valid for a homogeneous atmosphere only (i.e. at a constant altitude), but the parameters of N-wave can be computed by taking into account ambient conditions of temperature and pressure prevailing in altitude and at sea level [16]. Table 1 shows the result of simulations from JAZZ code compared to measurements of sonic booms from Apollo 15 and Apollo 16 flights: for every flight point the altitude and Mach number of which are specified, we give the ratio ΔP computed to ΔP measured for amplitude, and the ratio ΔT computed to ΔT measured for duration.

We can see that the error does not exceed ± 30 % for the amplitude ΔP and ± 10 % for the duration ΔT, with mean ratios close to one, which can be considered as a good result for a semi-empirical code, considering

Table 1. Comparisons calculation-measurements for Apollo's sonic booms.

US Navy ship	Altitude (m)	Mach number	Ratio of ΔPs	Ratio of ΔTs
USS Genesee	52,500	15.9	0.8	0.9
USS Ponchatoula	44,400	9.8	0.7	1.0
USS Kawishiwi	33,400	4.6	1.3	1.2
USS Okinawa	28,900	3.1	1.0	1.2
USS Ticonderoga	27,600	2.6	1.3	1.2
	Average ratio		1.0	1.1

the simplifications carried out (neither incidence nor lift effect). Note that here the "short-body correction" of Equation (4) plays an important role in the calculation of the N-wave duration.

3.2. Numerical approach

Geometry of Apollo Command Module and considered flight points

The Command Modules CM112 and CM113 of Apollo flights 15 and 16 are identical, but their precise geometry was not published. The Apollo 6 Command Module - geometry available in [17], including the radius of curvature at the junction of the spherical cap with the conical part (see Fig. 9) - well reproduces the characteristics of CM112 (Apollo 15) and CM113 (Apollo 16). Possible differences, of the order of 1 millimeter or 0.5 degree, will not act upon Navier-Stokes computations focused on the wake.

Two points of flight corresponding to the recorded sonic booms have been selected:

- for Apollo 15: z = 52.5 km, M = 16, T = 268 K, P = 58.4 Pa;
- for Apollo 16: z = 44.1 km, M = 9.6, T = 272 K, P = 186 Pa.

For the reentry of Apollo 16 Command Module, some meteorological measurements from instrumentation carried aboard a sounding rocket are given in [13]. For the Apollo 15 mission, we have based our argument on the US 1976 Standard Atmosphere model.

Preliminary analysis

In order to run Navier-Stokes computations, the essential point is to know the gas thermochemical state and the most appropriate physical model in order to describe such a state. According to the dissociation parameter, i.e. the product of upstream volumetric mass density ρ by reference length L_{ref}, one may foreknow that thermochemical state at the stagnation point by analogy with the study of R.N. Gupta et al. [18] about stagnation point on a sphere. Figure 10 shows the result of this analogy (the dissociation parameter is conserved): the studied cases Apollo 15 and 16 are both in a domain where the five chemical species are existing when the air is assumed in thermochemical equilibrium at the stagnation point.

Downstream, when the gaseous expansion is passing at the junction of the heat shield with the conical part and in the wake, these species can recombine occasionally, but the maximal number of species shall remain equal to five. However, it is not possible to assume that the flow remains at thermochemical

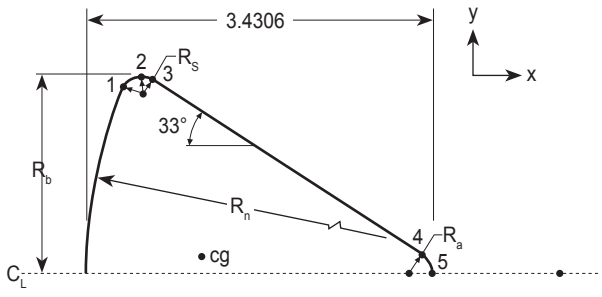

Location	x	y	s
1	0.3743	1.8368	1.8872
2	0.5543	1.9558	2.1158
3	0.6608	1.9242	2.2284
4	3.3254	0.1938	5.4056
5	3.3406	0.0000	5.6355
cg	1.1455	0.1600	–

D_b = 3.9116
R_b = 1.9558
R_n = 4.6939
R_s = 0.1958
R_a = 0.2311

Dimensions in m

Figure 9. Geometry of the Apollo 6 Command Module [17].

equilibrium downstream, because kinetics of chemical recombination achieves finite values. However, a set of adapted chemical kinetics can be selected (Park's 5-species model).

Axisymmetrical analysis

Although both Command Modules were stabilized along their trajectories by a highly negative incidence (angle of attack included between –22° and –20° at the considered points of trajectory), an initial step to determine the best model for the thermochemical state of the gas consisted of doing a preliminary study supposing that the flow was axisymmetrical (i.e. without incidence).

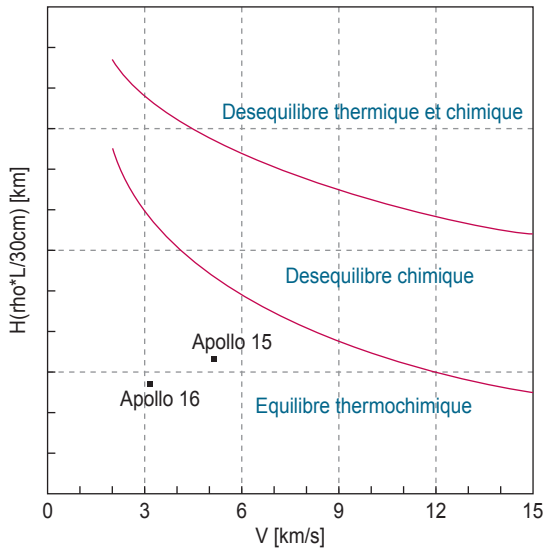

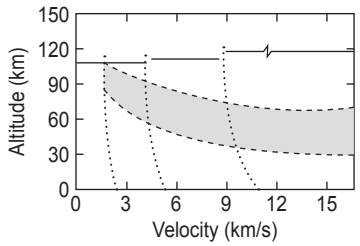

Chemical Species in Hig Temperature Air		
Region	**Air Chemical Model**	**Species Present**
I	2 species	O_2, N_2
II	5 species	O_2, N_2, O, N, NO
III	7 species	O_2, N_2, O, N, NO, NO^+, e^-
IV	11 species	O_2, N_2, O, N, NO, O_2^+, N_2^+, O^+, N^+, NO^+, e^-

Figure 10. *Thermochemical state of air at the stagnation point according to altitude, speed and aerodynamic parameters.*

The results of the Apollo 15 case are shown in Figure 11. We compare Navier-Stokes computations assuming that the 5-species air mixture is either at chemical equilibrium or at chemical nonequilibrium (finite rate chemistry).

The stagnation region is noticed to achieve the chemical equilibrium with a good approximation. However we also observe, from the very start of the reduction in pressure and all along the central part of wake, that the temperature is clearly less high in case of computation in nonequilibrium state than in case of equilibrium assumption. From this observation we infer that the rates of chemical recombination (it releases energy to the air flow) cannot be considered as infinite. In particular, it has a consequence on the shape of shock and on the pressure field which is represented as cross-sections in Figure 12.

Note that the turbulence in the wake is taken into account by a model of Spalart and Allmaras. It modifies neither the shape of the shock nor pressure profiles, consequently the selection of the model does not matter much, but this selection is necessary to stabilize the flow in the central region of the wake (see

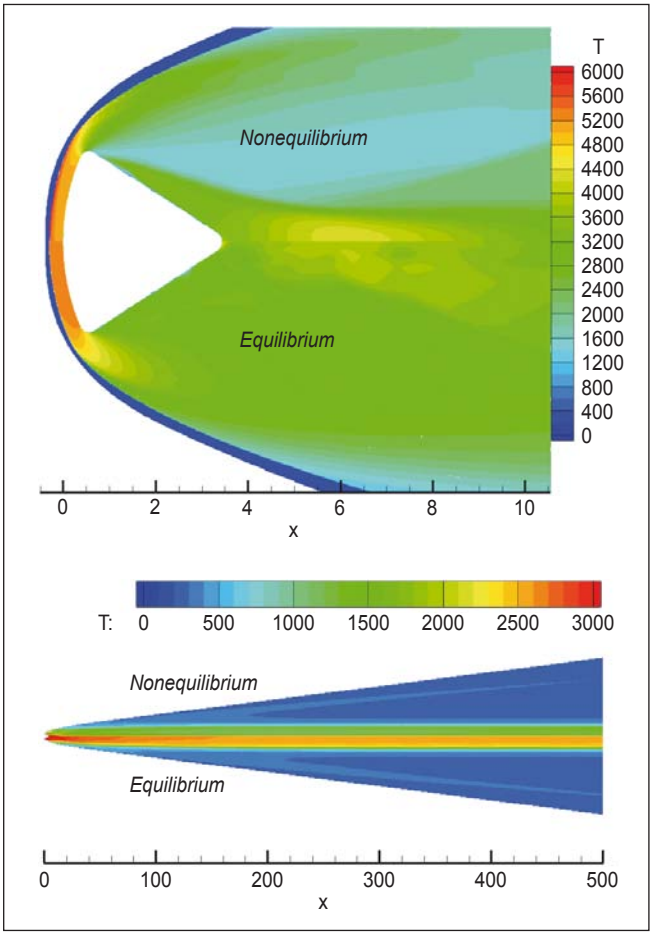

Figure 11. *Comparison between Navier-Stokes computations (chemical equilibrium vs chemical nonequilibrium).*

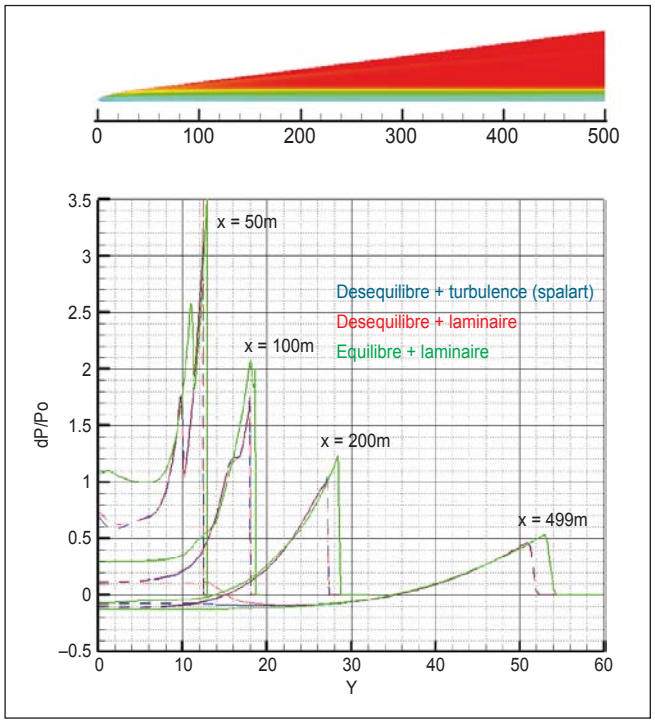

Figure 12. *Vertical cross-sections of wake in pressure.*

computation by half-wake in Figure 13). Moreover, Reynolds numbers achieved in the close and far wake increase sufficiently so as to admit, even considering a real gas hypersonic regime, there is established turbulence in this disturbed region. Note that the wake appears smoother in this case (Fig. 13, above).

Reconstructing of a sound source in 3D

The physical models selected could be identified in the cases of Apollo 15 and 16, as those of 5-species chemical equilibrium and 2-equations turbulence model. A 3D-mesh made up of parallelepipedic cells has been performed so as to catch the bow shock in the whole wake (for instance the location of the shock can be deduced by rotation from its position observed in axisymmetrical test case). Twenty six million cells

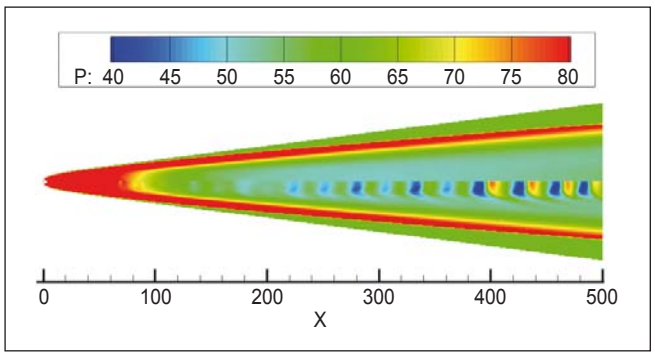

Figure 13. *Navier-Stokes computation: half-wake in turbulent case (above), in laminar case (below).*

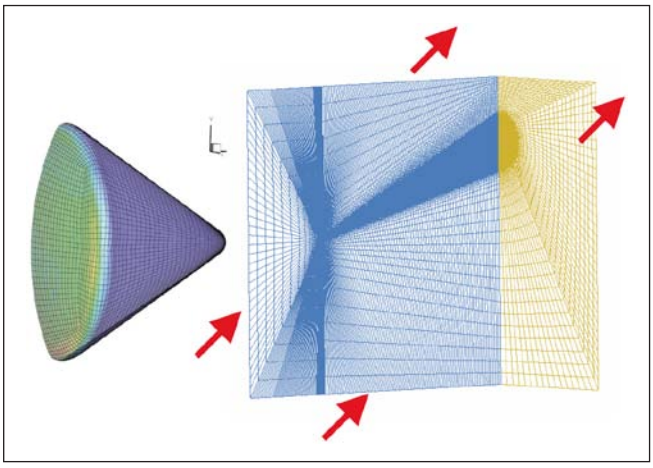

Figure 14. *3D mesh used for Navier-Stokes computations.*

were necessary to catch the hypersonic flow field for three kilometers downstream from Apollo 15 Command Module. Actually, because the shock is highly tilted at hypersonic speeds, this distance is mandatory if the far field assumption has to be respected accordingly with a sound propagation computation. But a shorter wake (500 m long) was employed for the Apollo 16 case, due to a smaller Mach number at a lower height.

Such highly meshed computations are extremely unusual for real gas in the hypersonic domain, focusing mainly on the flow in the vicinity of the vehicle rather than in its far wake.

Longitudinal profiles of pressure extracted from 3D calculations and used as input data into the sound propagation computations are displayed in Fig. 16. A significant discrepancy is then observed between the usual supersonic N-wave profile and the present

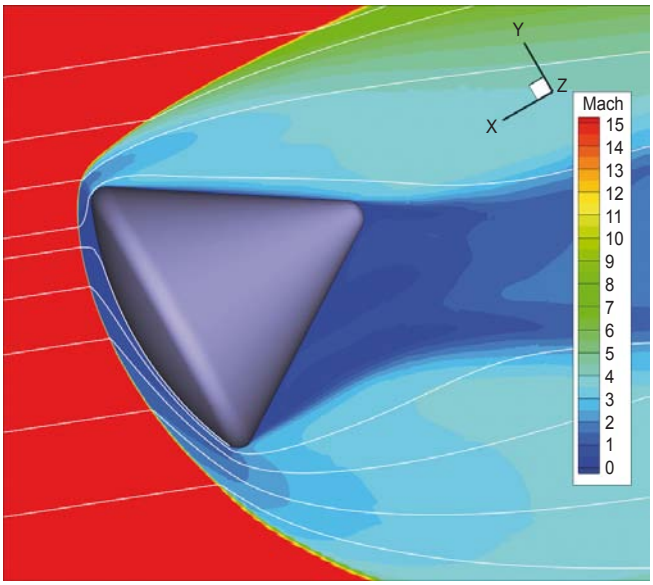

Figure 15. *Navier-Stokes computation assuming both turbulent flow and chemical nonequilibrium.*

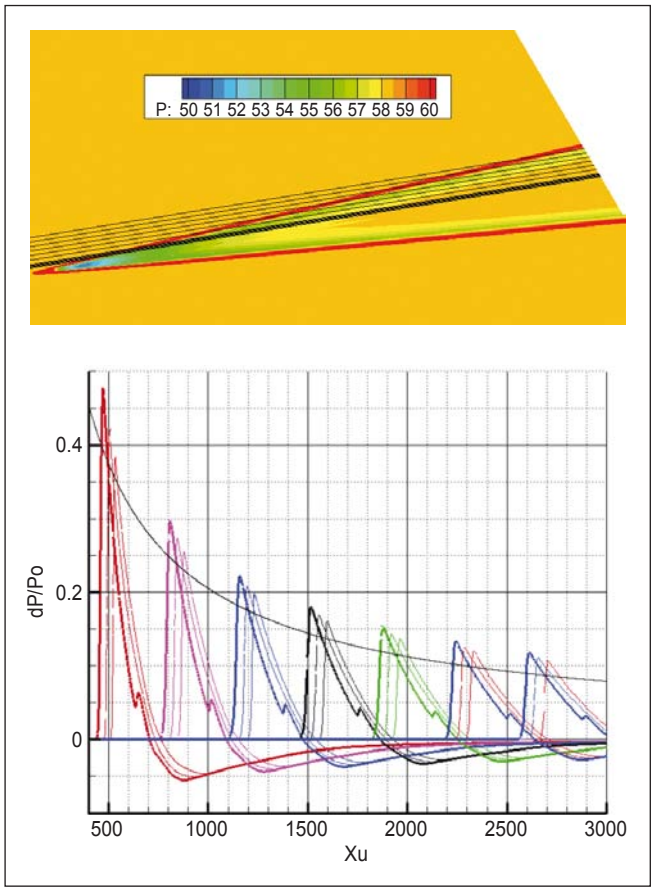

Figure 16. *Apollo 15, longitudinal pressure profiles computation.*

pressure profile, which tends towards the upstream value in an asymptotic way. Moreover, despite the high angle of attack and the expected 3D nature of the flow, the far-wake flow field is weakly asymmetrical regarding the pressure profiles.

Using the 20 m transversal profile (red curve in Figure 16) as input for the nonlinear propagation code TRAPS [15], we observe an intermediate shape of the propagated wave at first (Fig 17-1), then a return to the N-shape at sea level (Fig. 17-2). As a matter of fact, an intermediate shape was recorded actually (see Fig. 18), but this shape is also understandable by a wave reflected on the sea surface which arrives a small delay after the direct wave. The computation of Figure 17-2 provides the right global amplitude [$\Delta P^+ + \Delta P^-$], but it clearly overestimates the duration of the observed N-wave. We can think that the nonlinear propagation used is not well adapted to the physics of high atmosphere.

In Fig. 19 is represented the result of the simulation by means of the semi-empirical model JAZZ (see Table 1, line USS "Genesee"), by adding to the calculated N-wave another N-wave reflected on the surface of the sea, of same duration but of amplitude one half: indeed the reflected wave arrives on the sensors with a grazing incidence. The delay has been calculated by

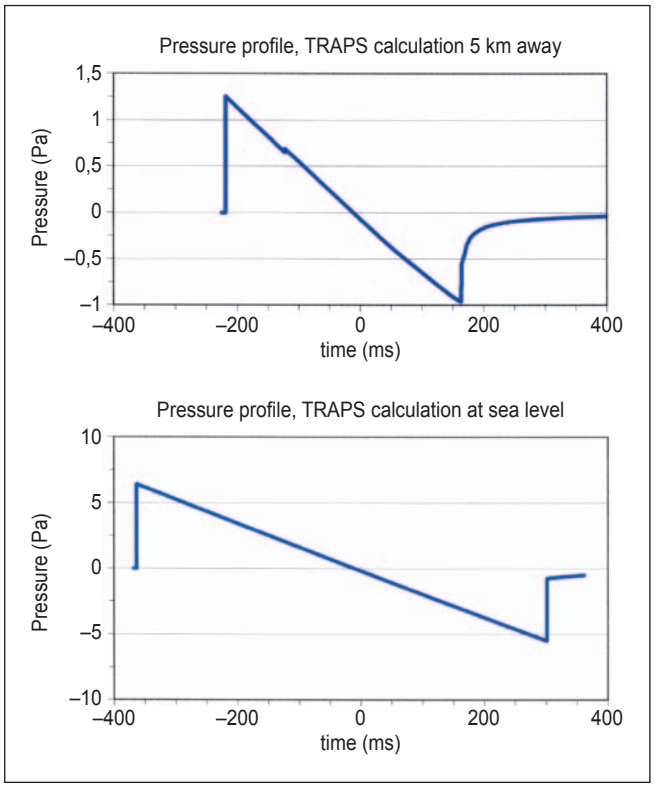

Figure 17. *Computed N-waves by the NASA's code TRAPS [15] at 5250 m from the Command Module (above) and at sea level (below).*

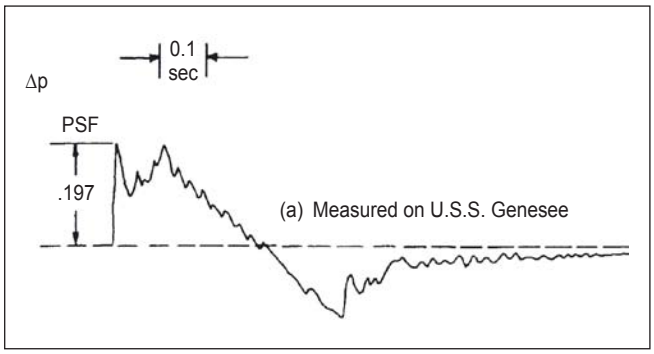

Figure 18. *Sonic boom from Apollo 15 flying at 52 km in height recorded at sea level [12].*

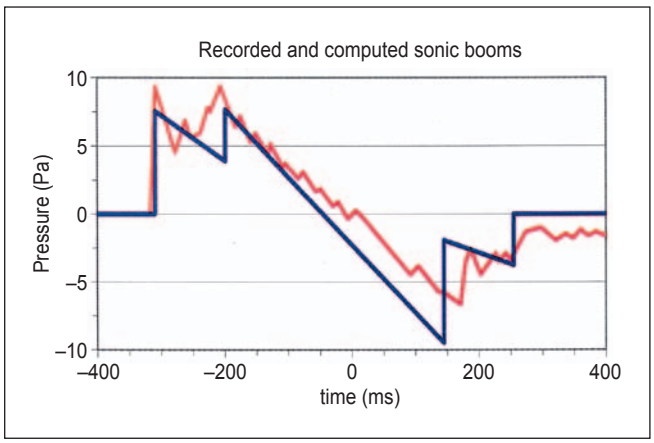

Figure 19. *Simulation of the signal received aboard USS "Genesee", by taking into account a sound reflection on the sea surface.*

taking into account the height of the ship, knowing that the sensors are put on the deck.

4. CONCLUSION

We showed two possible approaches in order to calculate a ballistic wave and a sonic boom. Our former approach requires classic models of semi-empirical type, while the latter requires heavy computation codes of fluid mechanics (CEDRE code) and of sound propagation (TRAPS code). In the latter case, a thorough study was carried out in order to found the physical approach that is the best adapted to high altitude. In the vicinity of Apollo Command Module, the CFD code CEDRE does not give a classical N-wave, but a half-alternation followed by an asymptotic return to the ambient pressure. At sea level, a nonlinear propagation restored a classic N-shaped profile with a correct amplitude, the duration of signal observed being overvalued.

It is interesting to notice that the semi-empirical model JAZZ can be utilized with success in the Apollo case, in spite of unusual conditions of height and speed for this type of model. For the N-wave duration, we apply a "short-body correction" which does not appear in the Whitham's theory. The simulation of the actual signal recorded at sea level can be improved by taking into account the sound reflection on the surface of the sea.

5. ACKNOWLEDGEMENTS

This work arises from the communication "L'onde balistique, de la balle de fusil au module Apollo" presented by J. Varnier and F. Sourgen (ONERA) during the French Congress of Acoustics CFA 2014, Poitiers, France, 22-25 April 2014.

The authors greatly appreciate Mr. Alexandre Alexieff, Consultant Engineer, for his helpful collaboration, as well as Dr. Jean-Luc Vérant, Head of Research Unit TACT, Dept. DMAE, ONERA, Toulouse, France.

6. BIBLIOGRAPHY

[1] E. Mach, *Photographische Fixierung der durch Projectile in der Luft eingeleiteten Vorgänge*, Akademie der Künsten und Wissenschaften, Vienna, (1887).

[2] P. Charbonnier, E. Esclangon, *Etude cinématique du champ acoustique d'un projectile. L'acoustique des canons et des projectiles*, Mémorial de l'Artillerie Française, tome IV, 3ème fascicule (1925).

[3] L.D. Landau, *On shock waves*, J. Phys. Acad. Sciences URSS 6, pp. 229-301 (1942).

[4] J.W.M. Du Mond, E.R. Cohen, W.K.H. Panofsky, and E. Deeds, *A determination of the wave forms and laws of propagation and dissipation of ballistic shock waves*, J. Acoust. Soc. Am., Vol. 18, No. 1, pp. 97-118 (1946).

[5] G.B. Whitham, *The behaviour of supersonic flow past a body of revolution, far from the axis*, Proceedings of the Royal Society of London, Serie A, 201, pp. 89-109 (1950).

[6] G.B. Whitham, *The flow pattern of a supersonic projectile*, Communications on pure and applied mathematics, Vol. V, No. 3, pp. 301-348, (1952).

[7] M. Schaffar, G. Parmentier, A. Dancer, M. Froböse, *Revue et synthèse de l'ensemble des travaux effectués sur le bang sonique, en particulier à l'ISL 1961-1974*, Rapport 40/74, Institut Saint-Louis (1998).

[8] S.R. Norris, E.A Haering Jr., and J.E. Murray, *Ground-based sensors for the SR-71 sonic-boom propagation experiment,* NASA TM 104310 (1995).

[9] L.G. Ivanteyeva, V.V. Kovalenko, E.V. Pavlyukov, L.L. Teperin, and R.G. Rackl, *Validation of sonic boom propagation codes using SR-71 flight test data*, J. Acoust. Soc. Am., Vol. 111, No. 1, pp. 554-561 (2002).

[10] R. Stoughton R., *Measurements of small-caliber ballistic shock waves in air*, J. Acoust. Soc. Am., Vol. 102, No. 2, Part 1, pp. 781-787 (1997).

[11] B.M. Sadler, T. Pham, L.C. Sadler, *Optimal and wavelet-based shock wave detection and estimation*, J. Acoust. Soc. Am., Vol. 104, No. 2, pp. 955-963 (1998).

[12] D.A. Hilton, H.R. Henderson, and R. Mc Kinney, *Sonic-boom ground-pressure measurements from Apollo 15,* NASA TN D-6950 (1972).

[13] H.R. Henderson and D.A. Hilton, *Sonic-boom ground-pressure measurements from the launch and reentry of Apollo 16,* NASA TN D-7606 (1974).

[14] J. Vallée, *Opération Jéricho-Focalisation. Mesure de l'intensité des bangs soniques engendrés par un avion volant en palier accéléré*, Rapport d'études N° 272 du Centre d'Essais en Vol (1967).

[15] A.D. Taylor, *The TRAPS sonic boom program,* NOAA TM ERL ARL-87, Air Resources Laboratories (1980)

[16] J. Varnier, *Sonic boom, jet noise and Doppler effect,* Acoustics in practice, EAA, Vol. 1, No. 2, pp. 7-15, (2013).

[17] *Apollo 6*, 9th AIAA/ASM Thermophysics and Heat Transfer Conference, San Francisco, CA (2006).

[18] R.N. Gupta, J.M. Yos, and I.A. Thompson, *A Review of Reaction Rates and Thermodynamic and Transport Properties for the Il-Species Air Model for Chemical and Thermal Nonequilibrium Calculations to 30,000 K,* NASA TM 101528 (1989).